Design of ground-layer turbulence compensation with a Rayleigh beacon

Andrei Tokovinin, Sandrine Thomas, Brooke Gregory, Nicole van der Bliek,
Patricio Schurter, Rolando Cantarutti, Eduardo Mondaca

Cerro Tololo Inter-American Observatory, Casilla 603, La Serena, Chile

ABSTRACT

The adaptive optics instrument for the SOAR 4.1-m telescope will improve the spatial resolution by 2-3 times at visible wavelengths, over a field of 3 arcmin, by sensing and correcting low-altitude turbulence selectively. We will use a Rayleigh laser guide star to accomplish this. We present the laser guide star design with predictions of system performance based on real turbulence statistics and telescope properties, sky coverage and some opto-mechanical aspects of the AO module. Various design trade-offs are discussed.

Keywords: Laser Guide Star, Adaptive Optics, Turbulence

1. INTRODUCTION

Progress of observational astronomy at all wavelengths is to a large extent driven by angular resolution. In the visible range, this is illustrated by the role that the Hubble Space Telescope (HST) plays despite its modest aperture. Large ground-based telescopes in the visible remain seeing-limited because the current generation of adaptive optics (AO) works mostly in the near-infrared.[1] Correction in the visible down to the diffraction limit is possible but restricted to a very small isoplanatic angle, bright laser guide stars (LGS) and natural guide stars (NGS), making AO almost useless for faint objects.

Ground-layer adaptive optics (GLAO) aims at enhancing the telescope resolution in a relatively wide field by correcting only low turbulent layers. Instead of reaching the diffraction limit, we only try to improve wavefront coherence at baselines of a few r_0. This leads to a significant resolution gain (compared to seeing) in a relatively wide field. GLAO can work in the visible and provides virtually complete sky coverage. For large (>4m) telescopes it has a potential to enhance the resolution and sensitivity to be of the same order as at HST. Recognizing the potential impact of GLAO, several teams are now considering its implementation.[2–4]

The 4.1-m SOAR telescope in Chile has been conceived and built with the idea of reaching the highest angular resolution by optimizing telescope quality and including tip-tilt compensation.[5] We are developing a GLAO system to further enhance SOAR capabilities. This paper presents the design of the SOAR Adaptive Module (SAM), including various trade-offs. SAM is based on existing and proven AO technology: the challenge of the project is in creating a useful and reliable instrument within a limited budget. The initial concept was described in Ref. 3. We also present a statistical estimate of the expected performance that quantifies the GLAO gain at the specific site, Cerro Pachón in Chile.

SAM will be a facility-class instrument, with a goal of making it simple and efficient despite the inherent complexity of LGS-assisted AO. Such an instrument will be a milestone on the development path of astronomical AO and will provide a firm basis for GLAO implementation at other large telescopes.

2. INSTRUMENT OVERVIEW AND PERFORMANCE

Major parameters of SAM are listed in Table 1. The current design is a result of numerous trade studies discussed further in Sect. 3. Figure 1 gives an overall opto-mechanical view of SAM and Fig. 2 presents a block-diagram of electronics.

Further author information: (Send correspondence to A.T.)
E-mail: atokovinin@ctio.noao.edu
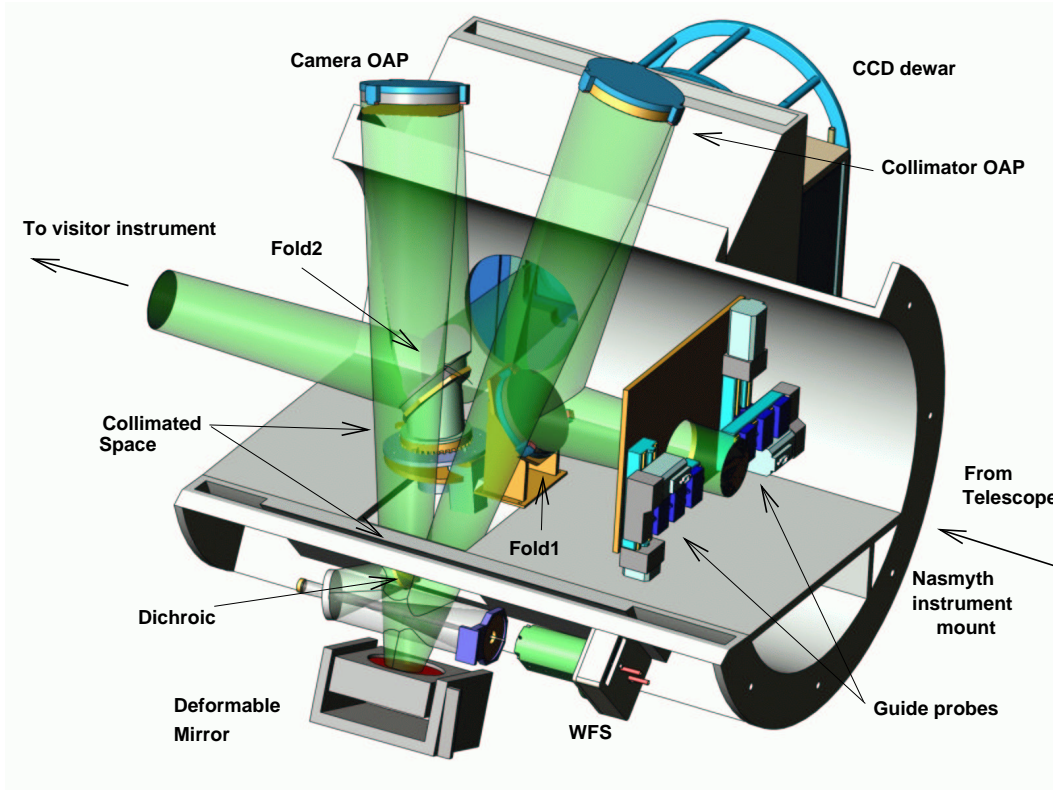
Figure 1. Overall view of the SAM instrument.

Table 1. SAM: major instrument parameters

Sub-system	Description
Deformable mirror	Bimorph BIM-60 (Cilas), pupil 50mm, 60 electrodes
Wave-front sensor	Shack-Hartmann 9x9, CCD-39, $0''35$ pixels in $3''$ sub-apertures
Re-imaging optics	Two OAPs $F = 810$ mm, off-axis shift 214mm
Laser	DS20-355 (Photonics), tripled Nd:YAG, $\lambda = 355$ nm, 8W, 10 kHz
Laser Launch Telescope	$D = 0.3$ m, reflecting, behind the SOAR secondary, $H = 10$ km
Range gating	KD*P longitudinal Pockels Cell + two $\lambda/2$ plates and polarizers
Tip-tilt guiding	Two probes linked by fibers to APDs, $R_{lim} = 18$
Focal plane	$3'$x$3'$ square field, $f/16.5$, scale 3 arcsec/mm, $R_{curv} = -0.9$m
Built-in CCD imager	4Kx4K, $0''05$ pixels, 6 filters
Collimated space	50-mm beam, 120mm along axis

The performance of a GLAO system with a single low-altitude Rayleigh LGS (RLGS) was evaluated by an approximate analytical method in Ref. 6. Several thousand low-resolution turbulence profiles for a continuous period of 21 nights at Cerro Pachón were obtained and processed to study the improvement of resolution expected from SAM. Representative results are given in Fig. 3.

The data in Fig. 3 refer to on-axis image quality. Further investigation[7] revealed that the anisoplanatism in GLAO is mostly caused by turbulent layers at altitudes between 0.5 and 1 km. In Fig. 4 (left) the worst-case situation is shown where 83% of the turbulence is at 0.5 km, the remaining 17% being located in high, uncorrected layers. Fortunately, the turbulence profile at Cerro Pachón displays a marked minimum at "difficult" altitudes
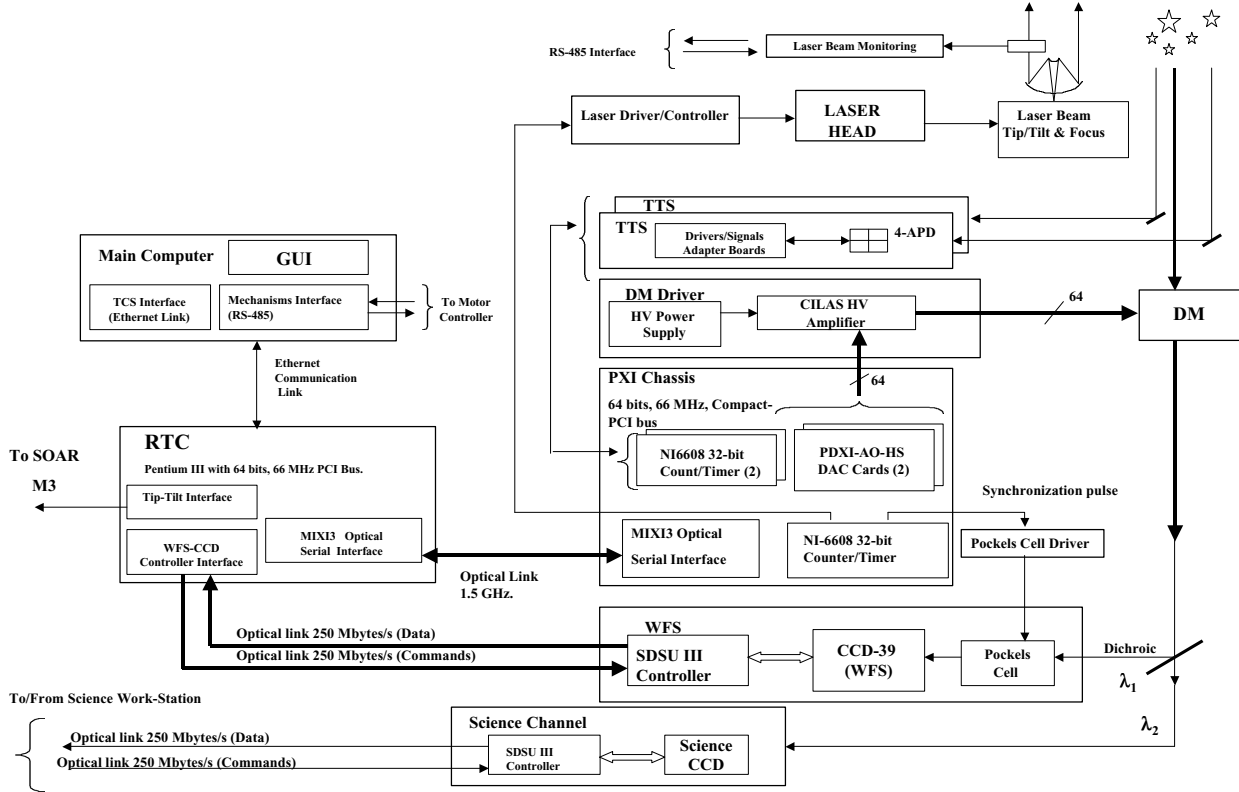
Figure 2. Block-diagram of the SAM electronics and component interactions.

from 0.5 to 2 km,[6] which means that a high degree of isoplanatism will frequently be reached over the whole 3′ field of SAM (Fig. 4, right).

3. DESIGN TRADE-OFFS

3.1. The laser guide star

Current concepts for GLAO (and for atmospheric tomography in general) are based on wave-front sensing with arrays of sodium or Rayleigh LGSs or, alternatively, with multiple NGSs. In terms of correction uniformity, a ring-shaped arrangement of sodium LGSs seems to be optimal.[7] This solution, however, is the most expensive one. NGSs, on the other hand, are restricted to magnitude 15 or fainter for reason of sky coverage. Hence, a GLAO system with NGSs will need sub-apertures of 1 m or larger and will correct the ground layer in the visible only partially, with a marginal gain. The complexity of NGS-based GLAO would be considerable because multiple re-configurable wave-front sensors (WFS) are required that will compete for visible light with the science detector.

Low-altitude Rayleigh LGSs were used in the 1st generation military AO systems. They were believed unsuitable for astronomical AO because of the cone effect. However, due to this same effect, low-altitude RLGSs preferentially sense ground-layer turbulence and are well-suited for GLAO. Even a single RLGS will be sufficient for a moderate-aperture telescope like SOAR. Operationally, it should be quite simple compared to the re-configurable multi-NGS option. The availability of rugged industrial solid-state lasers hints that a design of a simple "set-and-forget" RLGS may be achievable.

SAM will use an 8 W pulsed, frequency-tripled, Nd:YAG laser. Its short wavelength of 355 nm is doubly advantageous. First, the photon flux from Rayleigh scattering increases as λ^{-3} and, second, this radiation does
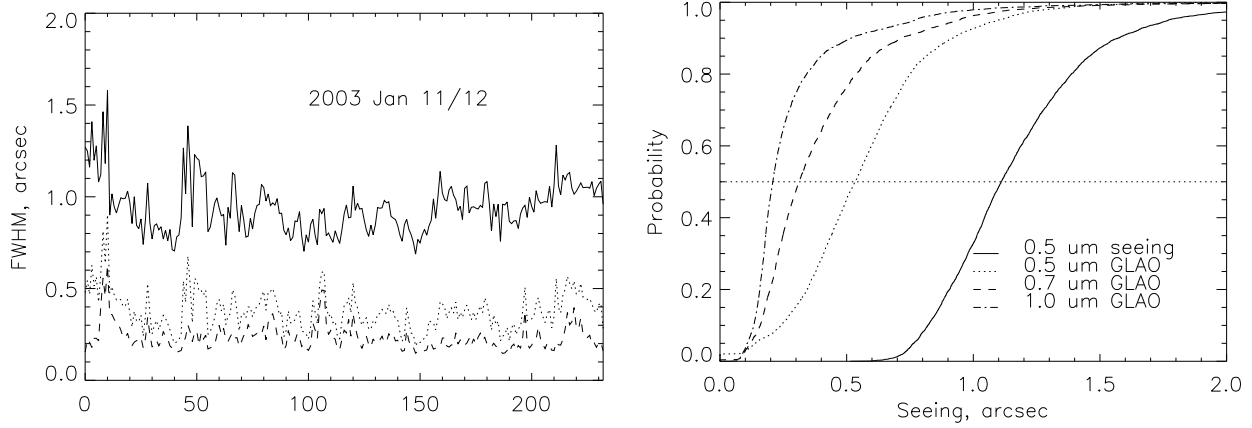
Figure 3. Left: Variation of the uncompensated image quality (full line) and GLAO-compensated quality at 0.5 μm (doted) and 0.7 μm (dashed) as a function of turbulence profile number (one profile per minute) on a typical night. **Right:** Histogram of the uncorrected seeing FWHM (full line) and of the SAM-corrected FWHM at 3 imaging wavelengths for the period of 21 nights in January 2003.
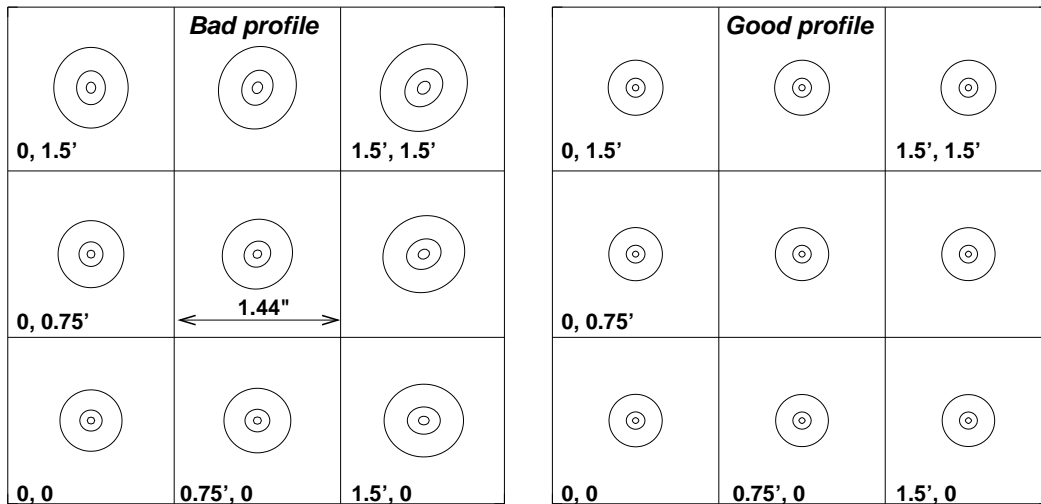
Figure 4. Mosaic of SAM-corrected PSFs at different positions in the field, starting from the center (lower left corner) to the outer (top right) corner. Each box is $1.''44$ on a side, the contours are at 0.1, 0.5, and 0.9 levels of the maximum. **Left:** unfavorable turbulence profile, **right:** good turbulence profile with 87% of turbulence below 0.5km. Both profiles correspond to the $0.''67$ seeing.

not present visual hazards. The UV RLGS is aircraft- and satellite-safe, obviating any need for coordination of AO observations with external agencies. The narrow laser beam on its way to the launch telescope needs to be shielded, but once it leaves the Laser Launch Telescope (LLT) it will be safe.

We computed the Full Width at Half Maximum (FWHM) β of the laser spots distorted by the ground-layer turbulence on upward and downward propagation (because of the beam convergence, only low turbulence effectively contributes to the image spread). The calculation includes the short-exposure atmospheric transfer function for a Gaussian beam on upward propagation, diffraction of this beam, and the same for downward propagation where a circular 0.5-m sub-aperture is assumed. The *effective* image size $\beta_e = \beta/\sqrt{T}$ takes into account the transmission T of the LLT resulting from the truncation of the Gaussian beam by its circular
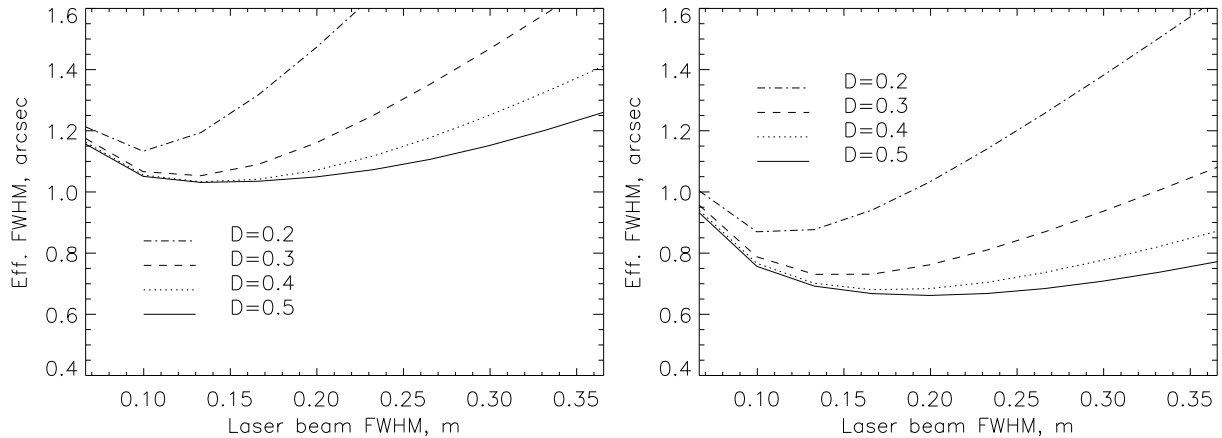
Figure 5. Effective laser spot size $\beta_e = \beta/\sqrt{T}$ as a function of the FWHM width of laser beam and the LLT diameter D. **Left:** expected average ground seeing $1''$, **right:** good ground seeing $0''.67$.

aperture (without central obscuration). We expect the centering errors in the WFS to be proportional to β_e, so this is is the parameter to minimize.

The results are shown in Fig. 5 for poor ground-layer seeing of $1''$ and for a more benign seeing. In the first case, the 30-cm diameter LLT with a FWHM of the laser beam around 0.13 m is close to optimum: a larger LLT brings little gain. The transmission will be $T = 0.8$. These parameters will also be acceptable under a better ground-layer seeing, although with a larger LLT the spot size could be further reduced by $\sim 10\%$.

By extrapolation from the published value of the return flux in RLGS AO system at Starfire Optical Range (Ch. 12 in Ref. 1) we estimate that the WFS will detect over 100 photo-electrons per sub-aperture per 2 ms loop time if the range gate is set to 150 m (spot elongation less than $0''.5$). Given the expected spot size of $1''$, a larger range can probably be selected.

The LLT will be located behind the secondary mirror of SOAR. This is the best position for many reasons. One of those is the effective blocking of the strong scattered signal from low altitudes. The entrance aperture of the WFS will not transmit the highly-defocused return beam because it will fall within the central obscuration zone. Only when the laser "bullet" is close to its nominal altitude around 10 km the light will enter the WFS. Even a moderate ($<10\%$) rejection ratio of the range-gate shutter will be sufficient for obtaining compact and high-contrast spots.

The secondary assembly of SOAR is relatively small and light (80 kg), which places tight constraints on the LLT design. We plan using a light-weight 30-cm mirror with a small secondary suspended on vanes. The primary will be actuated in tip, tilt and focus. The laser will be located on the upper surface of the telescope elevation ring. Its beam will be transmitted to the LLT over a distance of ~ 8 m with 2 or 3 reflections by flat mirrors. Owing to the relative stiffness of the SOAR tube (total flexure less than 0.5 mm), it will be possible to transmit the beam to LLT without controlling the tilts of those mirrors.

3.2. Which deformable mirror?

Successful implementation of a deformable secondary mirror at the MMT telescope[8] makes it an attractive option for AO in general and GLAO in particular. A Cassegrain secondary at SOAR is conjugated to 50 m below ground, but this mis-match will not be critical for a GLAO system with $3'$ field.

For reasons of cost and system complexity we selected for SAM the more conservative option of a small DM with re-imaging optics. Thus, SAM is a self-contained "adaptor" that delivers the corrected focal plane to a science instrument or to its own built-in imager.

Initially, we planned to use a small electrostatic DM from Okotech. A small DM leads to a smaller (and cheaper) instrument. Our study of the electrostatic DM[9] revealed that its stroke is barely sufficient to compensate median seeing. Considering that these DMs are fragile and provided only by single vendor, we finally selected a traditional, well-engineered bimorph DM from Cilas company. Bimorph DMs have ample stroke margin but larger pupil size (50-60mm). The AO instrument became bigger, but the incidence angles were reduced, facilitating the optical design.

3.3. Relay optics

The optical train of SAM from the telescope focal plane to the corrected focal plane includes 5 reflections and one dichroic (Fig. 1). The traditional optical design with off-axis parabolae provides diffraction-limited quality over the whole 3' square field. The field, however, has a radius of curvature about −900 mm, similar to the original SOAR focal plane. For GLAO, this curvature can be neglected because it produces only a small defocus of 0.″2. Two flat folding mirrors are introduced in order to constrain the overall instrument size. In addition, the second fold serves to switch the corrected beam between the CCD imager and the external "visitor" instrument.

The collimated space between the dichroic and the second fold is available for filters, grisms or Fabry-Perot etalons. The diameter of the collimated beam is 50 mm, but the diameter of the filter must be 70-100 mm if the whole 3' field is needed. The combination of high spatial resolution with spectroscopy is, generally, the most promising application of AO in astronomy. SAM is unique in offering the collimated space for user-defined spectral equipment. It will be a very efficient implementation of the AO spectro-imager, compared to a sequential combination of AO with 3D spectrograph.

A UV-reflecting dichroic directs the laser light to a very compact folded Gregorian WFS camera. We found that this design permits easy refocusing between the NGS at infinity and LGS at 10 km. Moreover, the optical quality and the output f-ratio are kept constant, facilitating WFS re-configuration. However, for NGS operation the dichroic will be replaced by a neutral beam-splitter.

3.4. Wave-Front sensor and range gating

In comparison with NGS-based AO, a RLGS relaxes the requirements for WFS sensitivity. Thus we select the proven Shack-Hartmann WFS principle. The 9x9 format matches the resolution of the DM and corresponds to a projected sub-aperture size of 0.5 m.

Our study[10] shows that the best pixel scale of the CCD should be approximately equal to the spot FWHM size. We thus select a CCD-39 chip with 24-μm pixels and a lenslet array with 192-μm pitch and focal length of 5.75 mm, with no re-imaging optics. This leads to a pixel size of 0.″375 and a field of 3″ per sub-aperture. With laser spots being no smaller than 0.″75, the pixels will be binned 2x2. With 4 output amplifiers and 500 Hz frame rate the pixel rate will be rather slow, 200 kHz, so that a readout noise of 3-4 electrons can be reached. Spot centroids will be calculated by cross-correlation with a suitable template,[10] ensuring the lowest possible centering error and linearity of the WFS.

A RLGS requires a fast electronic shutter in the WFS for range gating. Special fast CCDs with substrate gating capacity have been developed at MIT/LL for this purpose.[11] However, our literature survey indicates that these CCDs are less sensitive than CCD-39 at 355 nm: their quantum efficiency is around 0.4-0.5 (vs. 0.7 for CCD-39) and their noise is at least 5-6 electrons at comparable readout rate. Thus, we selected CCD-39 (which is used in other SOAR sub-systems, facilitating maintenance) with a Pockels cell shutter.

Pockels cells frequently serve as fast shutters in parallel laser beams. For a diverging beam with half-angle θ the rejection ratio of a cell of thickness x is degraded to $k = 0.005(x/2mm)^2(\theta/1.25°)^4$. This formula is valid for a KD*P crystal in a longitudinal cell (electric field parallel to the light beam) at wavelength 355 nm. We checked that alternative electro-optical crystals like BBO put tighter constraints on beam divergence because of their higher birefringence. In our WFS, $\theta = 0.7°$ for the "parallel" beam entering the lenslets, hence for a 4-mm thick crystal the rejection ratio is still good, $k = 0.002$. The cell can be also located near the focal plane of the WFS camera because the $f/40$ beam has $\theta = 0.7°$. The Pockels cell is placed between two crossed Glan-laser calcite prisms that block the light transmission until a 2.5 kV voltage is applied to the cell. The duration of the range gate pulse will be 1 μs (beacon vertical extent 150 m) or longer, subject to further optimization.

The laser beam is linearly polarized, but its polarization direction rotates with respect to the WFS because SAM as a whole rotates together with the Nasmyth bearing of the SOAR telescope. This difficulty will be circumvented by putting a $\lambda/2$ plate in the laser beam to convert it to circular polarization before launch. The return beam will be converted back to linear polarization by another $\lambda/2$ plate in the WFS. Thus, the rotation of the beam between two $\lambda/2$ plates becomes irrelevant.

3.5. Tip-tilt guiding
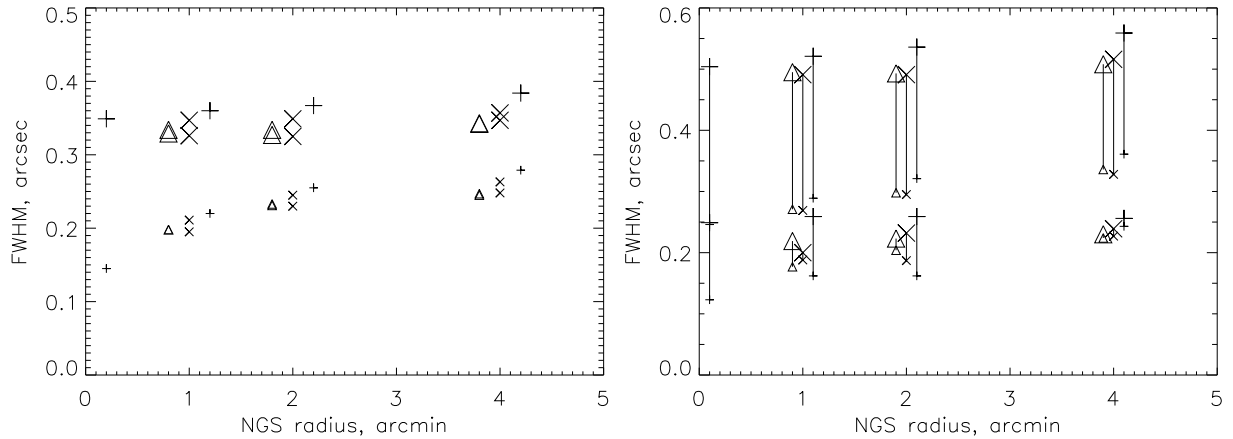
Figure 6. The FWHM at 0.7 μm versus number, configuration and radius of the tip-tilt NGS constellation. Triangles – 3 NGS, crosses – 2 NGS, pluses – 1 NGS. Small symbols show the best FWHM, large symbols - the worst FWHM. The horizontal axis corresponds to the radius of NGS configurations, with slight offsets. **Left:** Bad turbulence profile (lower layer at 0.5 km), all configurations. **Right:** Good (lower symbols) and worst (upper symbols) turbulence profiles, the best and worst FWHMs for each profile are connected by vertical lines.

AO systems with a LGS need tip-tilt (tt) sensing on a NGS. Usually, only one NGS is required. However, in a wide-field GLAO system the resolution will be degraded away from the NGS because of tt anisoplanatism. It is preferable to use several NGSs and average their tt signals to achieve a better PSF uniformity over the field. Using the tool described in Ref. 7, we studied the dependence of PSF uniformity on the number and configuration of tt NGSs. The turbulence profile corresponded to median seeing (0.″67 at 500 nm), with 17% of turbulence in high layers and 83% located at either 0 ("good"), 0.5 ("bad"), or 1 ("worst") kilometer above the ground.

In Fig. 6, we plot two points for each configuration, correponding to the smallest and the largest FWHMs over the field, respectively. The widths in x- and y-directions are considered. The difference in FWHM is thus a combined effect of anisoplanatism and PSF ellipticity. Quite naturally, the best correction at the field center is achieved for tight configurations of NGSs. The best possible PSF uniformity is reached for a NGS distance from the center of 2′ or more. Surprisingly, there is no penalty in selecting wider NGS configurations, hence the diameter of the search zone can be increased to 8′, with attendant increase of the sky coverage or of the NGS brightness. Also it is clear that 3 NGSs give little advantage, two NGSs being already sufficient. One NGS, as expected, leads to anisoplanatism.

SAM will contain two guide probes in the primary (uncorrected) focal plane. The tt compensation will be done by the SOAR fast tertiary mirror, as for the other science instruments. Thus, the DM is outside the tt loop and the tilts produced by the DM have to be small. The tilt modes will be filtered out from the high-order AO control.

The best resolution in GLAO will be of the order of 0.″2 – lower than in diffraction-limited classical AO and MCAO systems. Thus, the requirements for tt control are relaxed. A rms tt error of 27 mas is acceptable as it will degrade the central intensity of the PSF by no more than 10%. Our calculations show that with APD photon-counting detectors in a quad-cell tt sensor, a 30 mas rms error is reached for an $R = 18$ guide star with

a 3-dB servo bandwidth of 40 Hz. A much lower bandwidth (~ 10 Hz) is in fact needed for the compensation of atmospheric tt, but wind-induced telescope shake will likely require a fast tt servo.

The search zone of $8'$ diameter contains, on the average, 4 stars brighter that $R = 15.8$ near the Galactic pole. Only one star on each side of the $3'$ science field is actually needed. Thus, there is a convenient margin of at least 2 stellar magnitudes between the available tt stars and the faint limit of the tt guider. We are confident that the sky coverage of SAM will be nearly complete.

3.6. Mechanical design

Figure 1 gives a general idea of the mechanical design and packaging of SAM. The circular front flange will be installed on the Instrument Selector Box at the Nasmyth port of SOAR, while a science instrument will be mounted to the rear flange of SAM. The corrected SAM focus has the same f-number and scale as the original SOAR focus. The distance between the SAM flanges is 0.86 m.

By turning the second fold mirror, it will be possible to redirect the light to the built-in CCD imager. The shutter and filters of that imager will be copied from the existing SOAR imager design and will be interchangeable with the latter.

SAM has a small number of remotely controlled motions (x,y stages of the guide probes, fold-2, WFS focusing, laser focus and tip-tilt). All motions will be activated by intelligent motors on a common RS-485 bus. The motors will be un-powered when not in use in order to reduce the heat dissipation within the instrument.

The mechanical deformations of the SAM structure predicted by finite-element analysis are being taken into account in the optical model to assure the required image quality and stability. The alignment procedures are being considered from the beginning of the design, to make integration as easy and accurate as possible.

3.7. Computer and electronics

The choice of a Real-Time Computer (RTC) for the wave-front sensing and DM control is straightforward: a modern PC is several times faster than needed. The RTC will be located outside the dome. The signal from the WFS CCD SDSU-3 controller will be read via a fiber link to the PCI interface board. Other interfaces will be located in a PXI chassis near SAM. The latter will be connected to the RTC by another fiber that makes the PXI "transparent" to the RTC (Fig. 2).

3.8. Science instruments

SAM will contain a built-in CCD imager. This decision was taken because the regular SOAR imager is not available for AO-corrected focus, being located on the SOAR side-port. The SAM imager will be optimized for the red part of the optical spectrum where the SAM resolution gain is larger, while the regular SOAR imager works efficiently in the UV.

The second, "visitor" port of SAM will host the SOAR Integral Field Spectrograph (SIFS). The SIFS pixels are $0''.3$ square, so this instrument will greatly benefit from the improved light concentration provided by SAM: its magnitude limit for point sources will be extended by approximately 1^m.

In the future, other small specialized instruments can be placed at the visitor port. During the initial phase of SAM, when it will work without a LGS, a small high-resolution camera will occupy the visitor port, offering diffraction-limited resolution on bright targets that will also serve as guide stars.

4. SYSTEM ENGINEERING

Many current AO systems require the presence of the instrument team during observations. The challenge of SAM will be to hide the complexity of LGS-assisted AO and make observations as simple as possible, with the AO module being controlled by the telescope operator. A great deal of system engineering is needed here, some aspects are mentioned below. It is expected that this work will continue after the commissioning of SAM.

The laser is a rugged industrial model with a nominal time between failures of 8000 hours. No adjustments are required in normal use. The LLT will always point on telescope axis and will be focused at a fixed distance

of 10 km. Fine tuning of the LGS position on the sky will be done by a remotely controlled tip-tilt mirror in the LLT. We hope that a major part of the pointing error will be caused by elastic flexure and thus will be predictable. The WFS will acquire the LGS with a quick scan of the spot around its expected position.

NGS selection and acquisition for tt guiding will be automated. For each science pointing the software will select suitable stars from a catalog and will position the guide probes accordingly. Some spiral search will again be required, given the small $3''$ capture field of the probes, but the good pointing of the SOAR will facilitate this task.

Automatic AO loop optimization will be implemented. Covariances of the DM commands and WFS signals will be computed by the RTC in real time and used to estimate current atmospheric conditions. The command matrix will be regularly updated to ensure optimal AO performance without intervention of the operator. These data will also serve for predicting the compensated on-axis PSF. The degree of anisoplanatism can probably be evaluated using on-line data from the Cerro Pachón site monitor that incorporates a turbulence profile monitor, MASS.

The built-in turbulence simulator, TurSim,[12] will greatly facilitate the optimization of SAM, its control and maintenance. Most of the AO checking and tuning can be done during daytime. We hope to develop automatic procedures for instrument setup and checks.

Interaction with the SOAR will be a very important ingredient of achieving smooth operation. For example, pointing and focusing will be constantly offloaded to the telescope control system. An offsetting capability will be implemented where a shift of the telescope is accompanied by opposite shifts of guide probes, resulting in the offset of the science target on the detector.

REFERENCES

1. F. Roddier, ed., *Astronomical Adaptive Optics,* Cambridge Univ. Press, Cambridge, 1999.
2. R.G.M. Rutten, P. Clark, R.M. Myers et al., "Facility class Rayleigh beacon AO system for the 4.2-m William Hershel Telescope", *Proc. SPIE,* **4839,** pp. 360-369, 2003.
3. A. Tokovinin, B. Gregory, H. Schwarz, "Visible-light AO system for the 4.2-m SOAR telescope", *Proc. SPIE,* **4839,** pp. 673-680, 2003.
4. M. Chun, "Gains from a ground-only adaptive optics", *Proc. SPIE,* **4839,** pp. 94-106, 2003.
5. V.L. Krabbendam, T.A. Sebring, and S. Heathcote, "Southern Astrophysical Research Telescope (SOAR): steps on the road to success", *Proc. SPIE,* **4837**, pp. 71-81, 2003.
6. A. Tokovinin, "Ground layer sensing and compensation", *Proc. SPIE,* **5382,** 2004, in press.
7. A. Tokovinin, "Seeing improvement with ground-layer adaptive optics", *Publ. Astron. Soc. Pacif.,* 2004, in press.
8. F.P. Wildi, G. Brusa, A. Riccardi et al., "Toward first light of the 6.5-m MMT adaptive optics system with deformable secondary", *Proc. SPIE,* **4839,** pp. 155-173, 2003.
9. A. Tokovinin, S. Thomas, and G. Vdovin, "Using 50-mm electrostatic membrane deformable mirror is astronomical adaptive optics", *Proc. SPIE,* **5490**, paper 196, 2004.
10. S. Thomas, R. Cantarutti, "Optimized centroid computing in a Shack-Hartmann sensor", *Proc. SPIE,* **5490**, paper 123, 2004.
11. R.K. Reich, R.W. Mountain, W.H. McGonagle et al., "Integrated electronic shutter for back-illuminated charge-coupled devices", *Trans. IEEE Electr. Dev.,* **40,** pp. 1231-1237, 1993.
12. S. Thomas, "A simple turbulence simulator for adaptive optics", *Proc. SPIE,* **5490**, paper 162, 2004.